

Effect of molar ratio and concentration on the rheological properties of two-component supramolecular hydrogels: tuning of the morphological and drug releasing behaviour

Article

Accepted Version

Hansda, B., Mondal, B., Hazra, S., Das, K. S., Castelletto, V., Hamley, I. W. ORCID: <https://orcid.org/0000-0002-4549-0926> and Banerjee, A. ORCID: <https://orcid.org/0000-0002-1309-921X> (2023) Effect of molar ratio and concentration on the rheological properties of two-component supramolecular hydrogels: tuning of the morphological and drug releasing behaviour. *Soft Matter*, 19 (42). pp. 8264-8273. ISSN 1744-6848 doi: 10.1039/d3sm00883e Available at <https://centaur.reading.ac.uk/113851/>

It is advisable to refer to the publisher's version if you intend to cite from the work. See [Guidance on citing](#).

To link to this article DOI: <http://dx.doi.org/10.1039/d3sm00883e>

Publisher: Royal Society of Chemistry

All outputs in CentAUR are protected by Intellectual Property Rights law, including copyright law. Copyright and IPR is retained by the creators or other copyright holders. Terms and conditions for use of this material are defined in the [End User Agreement](#).

www.reading.ac.uk/centaur

CentAUR

Central Archive at the University of Reading

Reading's research outputs online

ARTICLE

Effect of molar ratio and concentration on rheological properties of two-component supramolecular hydrogels : Tuning of morphological and drug releasing behaviour

Received 5th July 2023,

Accepted 4th October 2023

DOI: 10.1039/d3sm00883e

Biswanath Hansda,^a Biplab Mondal,^a Soumyajit Hazra,^a Krishna Sundar Das,^b Valeria Castelletto,^c Ian W. Hamley,^c and Arindam Banerjee*^a

Self-assembled supramolecular hydrogels offer great potential as biomaterials and drug delivery systems. Specifically, peptide-based multicomponent hydrogels are promising materials due to their advantages that mechanical and physical properties can be tuned to enhance their functionalities and broader applications. Herein, we report two-component assembly and formation of hydrogels containing inexpensive complementary anionic, **BUVV-OH (A)**, and cationic **KFFC₁₂ (B)**, peptide amphiphiles. Individually, neither of these components formed a hydrogel, while mixtures with compositions 1:1, 1:2, and 2:1 (molar ratio) as **A:B** show hydrogel formation (Milli-Q water, at pH = 6.79). These hydrogels displayed a good shear-thinning behaviour with different mechanical stabilities and nano-fibrous network structures. The 1:1 hydrogel shows good cell viability for human embryonic kidney (HEK-293) cells and CHO cells indicating its non-cytotoxicity. The biocompatible, thixotropic 1:1 hydrogel with a nanofiber network structure shows the highest mechanical strength with storage modulus of 3.4×10^3 Pa. The hydrogel is able to encapsulate drugs including antibiotics amoxicillin and rifampicin and, anticancer drug doxorubicin, and it exhibits sustainable release of 76%, 70%, and 81% respectively *in vitro* after 3 days. The other two mixtures (composition 1:2 and 2:1) are unable to form hydrogel when they are loaded with these drugs. Interestingly, it is noticed that with an increase in concentration, the mechanical strength of a 1:1 hydrogel is significantly enhanced, showing potential that may act as a scaffold for tissue engineering. The two-component gel offers tunable mechanical properties, thixotropy, injectability, and biocompatibility and has great potential as a scaffold for sustained drug release and tissue engineering.

Introduction

Low molecular weight peptide-based supramolecular hydrogels have attracted considerable research interest over the last several decades.^{1–5} The formation of these hydrogels involves non-covalent interactions, including hydrogen bonding, π - π stacking, hydrophobic, electrostatic interactions, van der Waals interaction, and others.^{6–9} Furthermore, peptides can be designed to form hydrogels in response to various kinds of internal and external stimuli such as fuel^{10,11}, enzymes^{12,13}, pH¹⁴, temperature¹⁵, solvents¹⁶, metal ions^{17–19}, light, salt concentration, and these can also encapsulate specific drug or biological cargoes.^{20,21} Adams and co-workers have recently shown a new short peptide-based hydrogel with the variation of pH triggered by glucono- δ -lactone.²² Hydrogels

have been studied widely as soft materials due to their fascinating applications in different fields, including delivery and sustained release of encapsulated important biomolecules^{23,24} and drugs,^{25,26} tissue engineering,²⁷ regenerative medicine,²⁸ antibacterial activity,²⁹ 3D cell culture,³⁰ sensors,^{31,32} formation of nanocomposites,³³ catalysis in organic reactions,^{34,16} toxic dyes,^{35,4} metal ion removal from wastewater,^{35,4} and wound healing.³⁶ Smith and co-workers have developed the formation of gel tube by heating-cooling effect accompanied in the presence of salt.³⁷ Nowadays, synthetic peptides have been developed as flexible building blocks for forming hydrogels as they are made up of natural as well as non-natural amino acids and these gels can deliver metabolites with good tolerance and unique chemical properties. Besides, peptides can be tailored by changing the sequences of the amino acids, and hence these peptides spontaneously entangle to form fibrillar hydrogels, which show good biocompatibility to different kinds of cells and tissues.^{38,39} However, most of these hydrogels are homotypic, consisting of one type of building block, which puts a limit on the range of structural and functional complexities, tunabilities, and diversities.⁴⁰ On the other hand, multicomponent supramolecular hydrogels^{41–44} can be

^a School of Biological Sciences, Indian Association for the Cultivation of Science, 2A & 2B Raja S. C. Mullick Road, Jadavpur, Kolkata-700032. E-mail: bcab@iacs.res.in

^b School of Chemical Sciences, Indian Association for the Cultivation of Science, 2A & 2B Raja S. C. Mullick Road, Jadavpur, Kolkata-700032.

^c Department of Chemistry, University of Reading, Reading RG6 6AD, UK.

† Footnotes relating to the title and/or authors should appear here.

Electronic Supplementary Information (ESI) available: [details of any supplementary information available should be included here]. See DOI: 10.1039/d3sm00883e

prepared from: (1) two or more gelators which can either self-sort⁴⁵⁻⁴⁷ or co-assemble into different assemblies, (2) cooperative interactions between two components which are unable to form a hydrogel on their own, or (3) one or more peptide-based gelators and one or more non-gelling additives that can affect the co-assembly to form hydrogels.⁴⁸⁻⁵¹ This kind of co-assembly opens up a new window to explore a wide range of structural, functional, morphological, and mechanical properties of peptide-based hydrogels.^{40,52} The efficient means of having selective co-assembly is to introduce charged residues in place of neutral ones in the peptide sequence, where the opposite charges attract each other and like ones repel. It has been observed that ionic interactions in complementary peptides, peptide chain length, and hydrophobicity play a great role in the hydrogelation process, on their mechanical and physical properties.^{53,12} It has been found that heterotypic hydrogels (hydrogels made of more than one components) have some benefits over the homotypic hydrogels (hydrogels made of only one component).^{54,55} However, keeping all these facts in mind, herein, we designed and synthesized peptide-based two-component hydrogelators, component **A** (BUVV-OH) and component **B** (KFFC₁₂), and these two components are complementary to each other. Component contains a free carboxylic acid at C-terminal and **B** contains two free amines at N-terminal. In this study, we showed that none of the components form hydrogels on their own, but adding them together at different ratios (1:1, 1:2, and 2:1) leads to viscoelastic hydrogels that undergo shear thinning and recovery depending upon the nature of co-assembly. Among the three types of hydrogels, it was observed that the hydrogel at ratio 1:1 showed a greater storage modulus than others and the microstructure of this hydrogel consisted of nanofibers throughout the gel matrix. We further studied the variation of rheological property of the 1:1 hydrogel with the variation of the concentration of the hydrogelators. As concentration increases, the value of storage modulus increases by several times and thus, this may be useful in different applications not only in material science but also as biomaterials or biomedical materials. We investigated the hydrogels at different ratios of the two components **A** and **B** and characterized their structural features, mechanical properties, and biocompatibility using different techniques including ¹H NMR, FT-IR, rheology, SAXS, XRD, electron microscopy and cytocompatibility testing. Finally, we demonstrated slow and sustained release of drugs amoxicillin, rifampicin, and doxorubicin from the **A**:**B** 1:1 hydrogel with optimal rheological properties. We demonstrate ratiometric and concentration-dependent hydrogelation and drug release behaviour under tuneable conditions.

Experimental section

Materials and Methods

Materials: 11-aminoundecanoic acid (UNDA), L-valine (Val), L-lysine (K), L-phenylalanine (F), and dodecylamine (C₁₂) were purchased from Sigma-Aldrich. Thionylchloride, MeOH, NaOH, chloroform, N,N'-Dimethylformamide (DMF), formic acid, ethyl acetate, dicyclohexylcarbodiimide (DCC), di-tert-butylidicarbonate (Boc₂O), hydroxybenzotriazole (HOBT), aluminium oxide (basic), silica gel (100–200 mesh), and petroleum ether were purchased from SRL (India). Human embryonic kidney (HEK-293), Chinese Hamster Ovary (CHO), and MDA-MB 231 triple negative breast cancer cells were purchased from the National Centre for Cell Science (NCCS), Pune (India). Ultrapure water was in all experiments.

Peptide amphiphiles Synthesis and Their Characterization:

The all peptide amphiphiles are synthesized by standard solution phase methods by using racemisation-free fragment condensation strategy. The detailed synthetic procedures are provided in the Electronic Supplementary Information (ESI[†]). All the peptide amphiphiles were fully characterized by ¹H NMR spectroscopy, mass spectrometry, and ¹³C NMR spectroscopy. All NMR data were recorded on a Bruker DPX 500 MHz or Bruker DPX 400 MHz spectrometer at 300 K. Concentrations was in the range of 5 to 10 mM in CDCl₃ or DMSO-d₆. Electrospray-ionization mass spectra (ESI-MS) were obtained using a Q-ToF micro™ (Waters Corporation) mass spectrometer.

Morphological Imaging: The morphological properties of hydrogels were evaluated using field emission scanning electron microscopy (FE-SEM, JEOL-JSM-7500F), and high resolution transmission electron microscopy (HR-TEM, JEOL electron microscope at an accelerating voltage of 200 kV). For the FE-SEM the samples were prepared by drop casting 20 μl of gel sample (0.002% w/v) on mica foil. Samples for HR-TEM were prepared by drop-casting 10 μl aliquots on TEM grids (300 mesh Cu grids). In each case the drop-cast samples were dried under vacuum at 25 °C for 14 h. Then morphological images of the samples were obtained using the respective instruments.

FT-IR Study: A Nicolet 380 FT-IR spectrophotometer (Thermo Scientific) was used to obtain Fourier transform infrared spectra of xerogels.

Powder X-ray Diffraction (PXRD) Study: The powder X-ray diffraction data of the xerogel were recorded using a Rigaku SmartLab X-ray diffractometer operated at 9 kW (45 kV, 200 mA) using Ni filtered CuKα radiation and a 1D detector with scan speed 0.3 s and step size 0.02° over the range 2θ = 10–50°.

Small-Angle X-ray Scattering (SAXS) Study: Synchrotron SAXS experiments on solutions were performed on beamline B21 at

Diamond (Didcot, UK). Gel samples were loaded into a custom-designed gel sample cell.⁵⁶ Data was collected at 20 °C. The sample-to-detector distance was 3.71 m and the wavelength was 0.95 Å. The images were captured using a Pilatus 1M detector. Data processing (background subtraction, radial averaging) was performed using dedicated beamline software (ScÅtter).

Circular Dichroism (CD) Study: The circular dichroism spectra were recorded in a JASCO J-810 circular dichroism spectrometer at room temperature. Spectra were collected at a scan rate of 200 nm/s and 2 nm bandwidth from 200 to 500 nm with three times scans for averaging. Before running the sample, the baseline was corrected by the solvent. The solvent used here was ultrapure milli-Q water in which each sample was prepared.

General Procedure for Drug Release Study: For the drug release study, hydrogels incorporating amoxicillin, rifampicin, and doxorubicin were prepared. First, 1 ml of ultrapure water was used as the release medium. Then, 500 µl of the release medium was taken out at different time intervals to measure the UV absorbance. Release was monitored for 72h. The release efficiency was calculated as

$$\text{Release}(\%) = \frac{\text{release concentration}}{\text{loaded concentration}} \times 100$$

General Procedure for Cell Viability Assay Study: Cell viability was performed using a mitochondria enzyme dependent MTT [3-(4,5-dimethylthiazol-2-yl)-2,5-diphenyltetrazolium bromide] reduction assay (Mosmann, 1983). Human embryonic kidney (HEK 293), CHO (Chinese Hamster Ovary) and MDA-MB 231 triple negative breast cancer cells were seeded into 96 well plate at a density of 10⁴ cells/well treated with different concentrations of components (A and B) (0–250 µM) for 24 h. MTT (Himedia, India) was prepared at a concentration of 5 mg/ml in DPBS (Dulbecco's Phosphate-Buffered Saline) before use. A total of 100 µl of MTT (0.5 mg/ml) was added to each

200 µl of dimethylsulfoxide (DMSO) was added to each well to sufficiently dissolve the formazan precipitate. Cell viability was calculated by measuring absorbance at 570 nm using a microplate reader. Results were expressed as percentage of control:

$$\text{Cell viability}(\%) = \frac{\text{Abs.}(treated) - \text{Blank}}{\text{Abs.}(Control) - \text{Blank}} \times 100$$

Results and Discussion

Rationale of design and synthesis of two-component gelator

Herein, we successfully designed and synthesized a gelator containing two components by racemization free DCC coupling method in solution phase. One component (A) contains two amino acids (Val-Val) conjugated with Boc protected 11-aminoundecanoic acid (Boc-UNDA) at the N-terminal while the other (B) contains three amino acids (Lys-Phe-Phe) attached with a hydrophobic long chain dodecyl amine (C₁₂) at the C-terminal. In particular, A contains free α-carboxylic acid group at the C-terminus that confers hydrogen bonding as well as electrostatic interaction with the component B containing a free amino group at the N-terminal and a side chain amino group from the terminally positioned Lys residue. The synthesis details of component A has been given in a previously reported work.³ The peptide amphiphile B incorporates two aromatic moieties (Phe-Phe) and one long fatty acyl chain C₁₂ that can offer π–π stacking interactions and intercalation interactions, respectively. Moreover, there are two free α and ε amino groups of the lysine residue at the N-terminal of B that facilitate electrostatic interactions. We rationally designed the two component system to enable hydrogelation via these interactions. Here we show that they offer diversity not only in self-assembly behaviour, morphological and rheological properties but also in the drug release and cytocompatibility.

Peptide based two-component hydrogel formation

Molecular hydrogels were formed by mixing component A and component B. Component A shows acidic character due to the free carboxylic acid group at the C-terminal, while the component B is basic in nature due to presence of two free amino groups of lysine residue at the N-terminal (Fig. 1). The amphiphilic component A is soluble at physiological buffer (phosphate) solution (pH 7.46) as well as ultrapure water (pH=6.79) giving rise to a clear solution and does not form gels even after 30 days. On the other hand, B is sparingly soluble in these solvents and rather it forms a suspension which may be due to the presence of hydrophobic aromatic moieties (Phe-Phe) and along C₁₂ chain. Though both the components are complementary to each other, unexpectedly they do not form any kind of gel in the buffer solution by mixing them in any proportion. Interestingly, A and B form hydrogels at pH 6.79 by

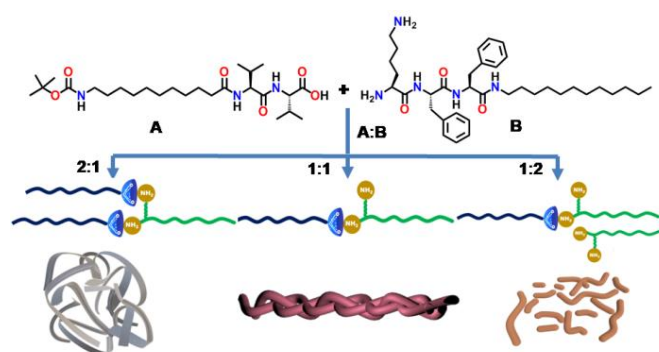


Fig. 1 Molecular structure of gelator molecules A and B, and schematic diagram of their assembly pattern in different ratios.

well. The cells were incubated at 37 °C and 5% CO₂ humidity for 4 h. After incubation, the MTT solution was aspirated and

heating and cooling method. In this study, we combined these two components at the ratio of 1:1, 2:1 and 1:2 (molar ratio **A:B**) that give rise to hydrogels of different strength and appearance in nature. The hydrogel formation procedure does not involve harsh conditions or pH adjustment. Thus, in the simplest way, we formed two-component hydrogels and proceed further for various experimental studies and applications.

Understanding of rheological behaviour of the hydrogels at different ratios

Rheology is an essential experiment to understand the viscoelastic character and microstructural behaviour of hydrogel. The information obtained from the experiment can analyze the deformity and recovery behaviour of hydrogels used in various practical applications (like tissue engineering, controlled release of drugs and biomolecules, 3D-cell proliferation, etc.). Using oscillatory shear measurements of dynamic mechanical properties, a frequency sweep experiment was carried out at a constant strain % of 0.05% with frequency ranges from 0 to 100 rad/s at ratio of **A:B** = 1:1, **A:B** = 1:2 and **A:B** = 2:1. From the data in Fig. 2 it is clear that all these hydrogels have greater storage modulus (G') than loss modulus (G'') and with weak frequency dependence over the measured range. The fact that $G' > G''$ shows the solid-like character of the hydrogels. The 1:1 hydrogel (Fig. 2a) shows a higher storage modulus than those of the 1:2 or 2:1 hydrogels (Fig. 2b or Fig. 2c) though the G' value for the 1:2 hydrogel is slightly lower than for the other two hydrogels.

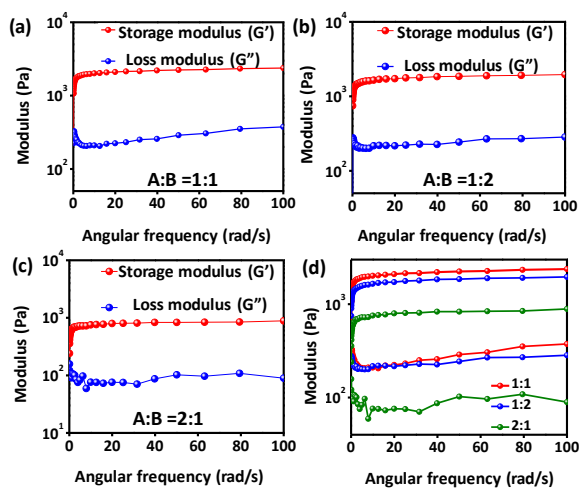


Fig. 2 (a-c) Frequency sweep experiment of the two-component hydrogel at different ratio of **A** and **B** at a constant strain of 0.05%. (d) Stacked format of the three hydrogels for the clear view of appreciate differences among frequency sweep results.

The appreciable differences of the modulus of these hydrogels are clearly shown in the stacked plot in Fig. 2d. However, this observation can be attributed to the fact that the hydrophilic/lipophilic balance is optimal for the 1:1 hydrogel.

Detailed Rheological analysis and thermal effect on hydrogels

Components **A** and **B** form hydrogels at three different ratios i.e., at 1:1, 1:2 and 2:1. Among them 1:1 hydrogel showed the highest storage modulus, G' . However, to get better insight into the rheological behaviour of 1:1 hydrogel we further performed concentration- dependent frequency sweep and time sweep experiments. These experiments are essential to characterize properties that are essential for slow drug release, tissue engineering, cell proliferation, and wound healing. To investigate the role of concentration of the hydrogelator, six sets of hydrogels were prepared by varying concentration from 0.3% w/v (above MGC = 0.25% w/v) to 2% w/v. The variation of storage modulus G' and loss modulus G'' of the 1:1 hydrogel at different concentration in the frequency range of 0.1–100 rad/s is illustrated in Fig. 3. As expected, due to the better entanglement of the fibrillar network of the hydrogel G' and G'' values increases significantly with increasing concentration of the gelators, indicating the enhanced mechanical strength and stiffness of the hydrogels. For all the concentrations it was observed that the hydrogels exhibited viscoelastic behaviour ($G' > G''$) throughout all the frequency ranges accompanied by good linearity. The increase

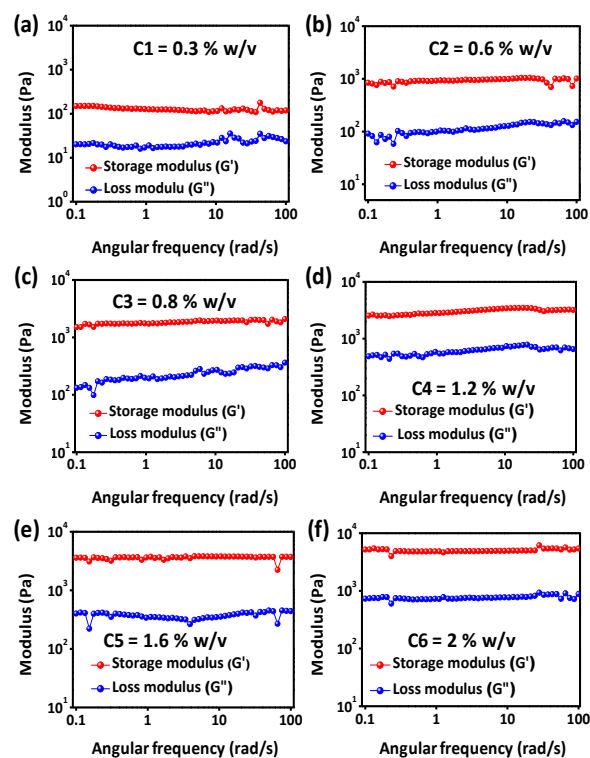


Fig. 3 (a-f) Frequency sweep experiment of the two-component hydrogel (**A:B** = 1:1) at different concentration at a constant strain of 0.05%.

in G' values of the hydrogels is notable for all the concentrations. The most rapid increments of G' values were observed at lower concentration (Fig. 3a-c). Fig. S4 (ESI[†]) shows a plot of G' against concentration, clearly a gradual variation of G' with the increasing concentration. We also

probed the effect of temperature on the different types of hydrogels and measured the gel-to-sol transition temperature designated as T_{gel} . Here, it was observed that the 1:1 hydrogel (0.3% w/v) showed the highest T_{gel} value which was about 75 °C. It was 72 °C for the 1:2 hydrogel and for 2:1 hydrogel it was 68 °C. Furthermore, the dependence of T_{gel} on concentration was determined and it was found that T_{gel} also increases with concentration (for 1:1 hydrogel). For the increment of concentration from 0.3% to 2% w/v the T_{gel} increases from 75 °C to 94 °C (1:1 hydrogel). Here it was observed from the plot of T_{gel} versus concentration, the T_{gel} increases nearly linearly with the increase in gelator concentrations (Fig. S5, ESI†).

To evaluate the microscopic recovery properties of the hydrogels, cyclic strain sweep experiments at different concentrations were performed for the 1:1 hydrogel. Strain-dependent rheological measurements revealed the shear thinning and recovery properties of the 1:1 hydrogel. These hydrogels were in were stable over a range 0-18% strain, whereas after that these turned into solution state (Fig. 4a-f). The three intervals of thixotropic test (3iTT) were carried out at constant strain amplitude value of $\gamma_{low} = 0.05\%$ and $\gamma_{high} = 30\%$ at constant frequency 1 rad/s for 0.3% w/v, 0.6% w/v, 1.2% w/v, 1.6% w/v and 2.0% w/v hydrogels whereas it was $\gamma_{low} = 0.1\%$ and $\gamma_{high} = 40\%$ for the 0.8%w/v hydrogel. Under the condition γ_{low} , the gel form was stable over an extended observation period, but applying γ_{high} the hydrogels were disrupted to give solutions. After removal of applied γ_{high} the gel state was recovered. This gel-sol transformation was observed for several cycles of applied strain. For better understanding of this cyclic transformation two parameters, deformation percentage (%D) and recovery percentage (%R) were evaluated between two γ states (γ_{low} and γ_{high}) using the formulae as shown in eqn. 1.

$$\%R = \frac{G'_x}{G'_i} \times 100 \quad \%D = \frac{G'_i - G'_x}{G'_i} \times 100 \quad (1)$$

Where G'_i is the storage modulus at the end of the first step and G'_x is the storage modulus value of the next step at which large amplitude strain was applied, $x = 3, 5, \text{ and } 7$ and so

Table 1: List of values of %R and %D for 1:1 hydrogel

Steps	% R at different concentration			% D at different concentration		
	0.3% (W/V)	0.6% (W/V)	0.8% (W/V)	0.3% (W/V)	0.6% (W/V)	0.8% (W/V)
Third step	98.74	90.74	99.45	1.26	9.26	0.55
Fifth step	97.48	85.65	98.98	2.52	14.35	1.02
Third step	1.2% (W/V)	1.6% (W/V)	2% (W/V)	1.2% (W/V)	1.6% (W/V)	2% (W/V)
	80.89	93.27	98.10	19.11	6.73	1.90
Fifth step	75.54	84.76	95.72	24.46	15.24	4.28

on. It was observed for hydrogels containing 0.3 – 0.8% (w/v) peptide that, although there is no regularity in recovery of storage modulus (G') after withdrawing γ_{high} , there is good recovery of G' in the third step. The values of %R and %D are tabulated in the table 1. The %R and %D values in this step are 98.74, 90.74, 99.45 and 1.26, 9.26, and 0.55% consecutively. In the fifth step slight decrease in recovery was observed and the values are obtained as 97.48, 85.65, 98.98% and 2.52, 14.35, and 1.02% sequentially. On the other hand, for 1.2% w/v hydrogel to 2% w/v hydrogel the recovery in G' values are gradually increasing that correspond to the values of 80.89, 93.27, 98.10% and 19.11, 6.73, and 1.90% consecutively for %R and %D in the third step. As expected for the fifth step, the values were slightly lower in magnitude which corresponded to 75.54, 84.76, 95.72, and 24.46, 15.24, and 4.28% consecutively for %R and %D respectively. These results indicate that the hydrogels are composed of nanostructured networks that are able to re-gel during the three intervals of thixotropic test (3iTT). The recovery properties are good and are not greatly influenced by concentration.

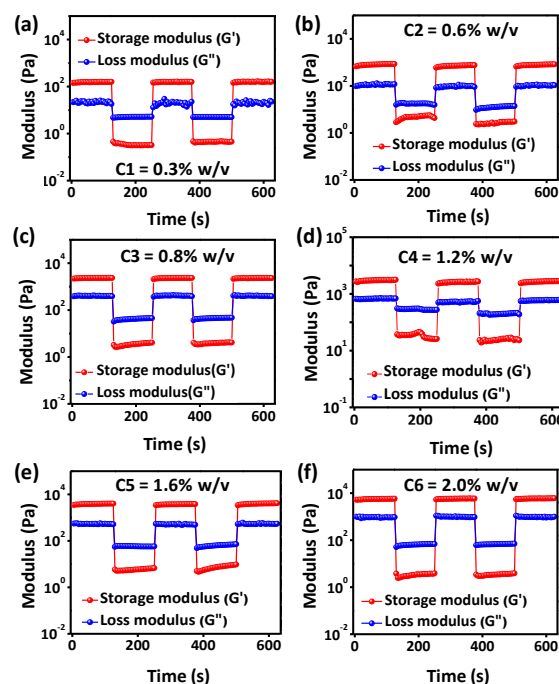


Fig. 4 (a-f) Time sweep experiment of the two-component hydrogel (A:B = 1:1) at different concentration.

Plausible mechanism of gel formation: (FT-IR, NMR)

Supra-molecular self- and co-assembled hydrogel formation can be driven by a diverse number of factors depending upon various types of stimuli. Hydrogen bonding may be an important driving force leading to hydrogel formation, and this can be probed directly by Fourier transform infrared (FT-IR) spectroscopy. The FT-IR data were evaluated for powders and xerogels for the three mixtures of A and B. Fig. 5 shows the characteristic peaks of hydrogen bonding as well as others associated with hydrogelation. The component A and B

exhibited different vibrational bands at 1650 and 1645 cm^{-1} respectively that are attributed to the amide I stretching vibrational bands of the respective components (Fig. 5a,b). On the other hand, the peaks at 1520 and 1544 cm^{-1} signify the amide II stretching vibrational peaks of the same two components. However, in comparison to the vibrational bands of **A** and **B** the peaks for xerogels appear at 1632 and 1538 cm^{-1} (for **A**:**B**=1:1, Fig. 5c), 1637 and 1541 cm^{-1} (for **A**:**B**=1:2, Fig. 5d), and 1638 and 1548 cm^{-1} (for **A**:**B**=2:1, Fig. 5e). All these vibration bands showed shifted values with respect to the individual components and hence the changes may be attributed to the contribution of amide groups in hydrogen bonds. Most importantly the peak at 1724 cm^{-1} clearly indicates the -C=O stretching frequency of carboxylic acid group of **A** which is absent in **B**. In all xerogels the peak disappeared and red shifted to 1681, 1682 and 1683 cm^{-1} for 1:1, 2:1 and 1:2 respectively, suggesting the strong interaction of carboxylate group of **A** and amine group of **B**. Peaks are observed at around 2920 and 2852 cm^{-1} for all the cases indicate the asymmetric and symmetric stretching vibrations

However, the peak for the carboxylic acid of component **A** appeared at $\delta = 12.52$ ppm (Fig. S6). It was clearly observed that the peak completely disappeared in the spectra measured for all three mixtures. This clearly indicates the formation of carboxylate ions that interact with the amine group of the component **B**. Thus, from FT-IR and ^1H NMR, it can be concluded that amide protons of each of the component participated in the intermolecular hydrogen bond ($\text{N-H}\cdots\text{O}$) which is an important driving force leading to hydrogelation. Interionic interaction between component **A** and **B** also played a significant role in the co-assembly giving rise to formation of two component hydrogel. The π - π stacking between aromatic moieties (data from PXRD, to be discussed shortly) had great contribution to immobilize the large amount of solvent molecules to form hydrogel.

Morphological Studies

The morphological study of co-assembled structures of two-component hydrogels at different ratios is an essential characteristic to be discovered to obtain an insight into structure due to co-assembly. HR-TEM and FE-SEM studies were performed to get the detailed structural features of the hydrogels. These show that the variation of the ratio of the components **A** and **B** does influence to some extent the morphology of these hydrogels. From the TEM images, it is observed that the hydrogel at ratio **A**:**B** = 1:2 appears to comprise discrete nanofibrillar structures (Fig. 6a). Both short and long fibers are observed. This type of distribution of the morphology of the hydrogel (**A**:**B** = 1:2) may be attributed to the fact that half of the component **B** interacts with component **A**, giving rise to long fibrillar structures *via* co-assembly. On the other hand, we propose that the other half of component **B** forms short fibres due to self-association. In the case of ratio of **A**:**B** = 1:1, we observe fibres that are straight, long ranged, and entangled into a comparatively homogeneous coiled structure (Fig. 6b). The 1:1 hydrogel comprises a more uniform fibril morphology due to co-assembly in the mixture with matched composition. This in turn provides more stability to the hydrogel assessed by rheology measurements (discussed above). Finally, the hydrogel, **A**:**B** = 2:1, (Fig. 6c) exhibits ribbon-like nanostructures. The appearance of this type of morphology

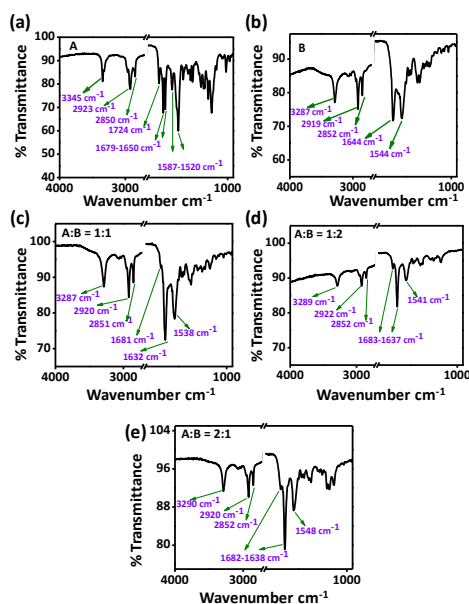


Fig. 5 FT-IR spectra of powder of (a) **A**, (b) **B** and xerogels of their mixture at different concentration (c) **A**:**B** = 1:1 (d) **A**:**B** = 1:2 and (e) **A**:**B** = 2:1.

respectively for the CH_2 groups in the lipid chains. Moreover, peaks ranging from 3345 to 3287 cm^{-1} of individual components as well as xerogels also signify presence of N-H hydrogen bonding which contribute to the self assembly of the components and hydrogel formations of the mixture.

To get further insight about the intermolecular interactions involved in the process of gelation, we performed ^1H NMR analysis in DMSO-d_6 solvent to observe changes in chemical shift (δ in ppm). We first recorded NMR data for the individual components, **A** and **B**. Then the NMR data of the components at the particular ratio (0.5% w/v) were measured. Though there was no prominent chemical shift in the aromatic region, a very low shift was observed in the amide N-H region.

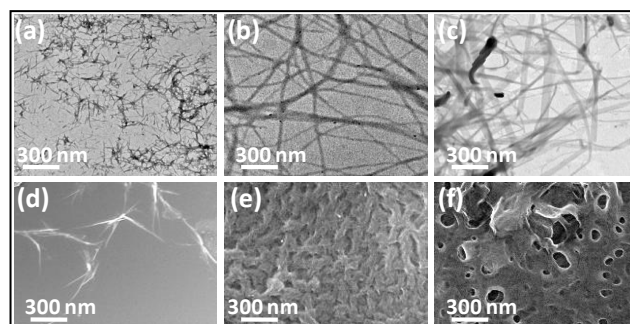


Fig. 6 HR-TEM images of the hydrogels (a) **A**:**B** = 1:2, (b) **A**:**B** = 1:1, (c) **A**:**B** = 2:1 and FE-SEM images of the corresponding hydrogels (d-f).

may be attributed to the predominant nature of component **A**. Fig. 6d-f show FE-SEM images of the corresponding hydrogels. These provide support to the assignments of morphology obtained from the HR-TEM images.

Structural Studies

To elucidate the molecular packing within co-assemblies, SAXS measurements were performed on native hydrogels, while PXRD was performed on their respective xerogels. For the 1:1 and 1:2 hydrogels, the d-spacing from SAXS were 47 Å and 48 Å (Fig. S7a, b). In the case of 2:1 hydrogel no significant SAXS signal was obtained. Fig. 7 shows the PXRD data of xerogels prepared from mixtures at different molar ratios. For the xerogel of ratio **A:B** = 1:1 (Fig. 7a) sharp peaks are observed at $2\theta = 9.68^\circ$ and $2\theta = 19.99^\circ$ corresponding to the d-spacing values of 8.89 and 4.32 Å respectively. The d-spacing value 8.89 Å is assigned to β -sheet structure, and the value 4.32 Å indicates the presence of hydrogen bond between gelator molecules in the xerogel state. Another important peak at $2\theta = 22.68^\circ$ with d-spacing 3.81 Å is due to the presence of extensive π - π stacking between aromatic groups that participate in co-assembly to form gels. For the xerogel **A:B** = 2:1 (Fig. 7b) the only peak observed was that at $2\theta = 19.68^\circ$ accompanying d-spacing of 4.48 Å, due to hydrogen bonding. In the case for the xerogel of ratio **A:B** = 1:2, (Fig. 7c) the diffraction peaks were detected at $2\theta = 7.65^\circ$, 9.46° , 18.55° , 20.12° and 21.91° corresponding to d-spacing values of 11.24 Å, 9.09 Å, 4.65 Å, 4.29 Å and 3.94 Å respectively. From the d-spacing values, it can be concluded, for this instance, that the molecular stacking arrangements are of similar type with the xerogel of ratio **A:B** = 1:1, i.e. β -sheet (d-spacings 11.24 Å, 9.09 Å, 4.65 Å, and 4.29 Å), hydrogen bonding, and π - π stacking (d-spacing 3.94 Å). The observed d-spacing values for β -sheet structure of **A:B** = 1:2 xerogels implies that there may be two types of assemblies that are present, as shown by HR-TEM and HR-SEM (Fig. 6a,d). It is proposed that half of the molecules of **B** form β -sheet-like structure in the co-assembled form with component **A**,

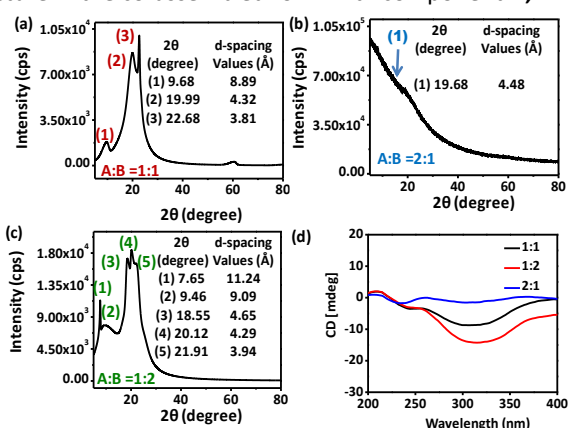


Fig. 7 Powder XRD spectra and data of the hydrogels (a) **A:B** = 1:1, (b) **A:B** = 2:1, and (c) **A:B** = 1:2. (d) Circular dichroism spectra of the hydrogels of **A:B** = 1:1 (black), **A:B** = 2:1 (blue), and **A:B** = 1:2 (red).

whereas the other half of **B** are self-assembled giving rise to a β -sheet structure with a different d-spacing. Additionally, more

evidences about the structural properties can be obtained from the circular dichroism (CD). From the Fig. 7d it was observed that the CD spectra contained positive maximum around 210 nm and negative maximum around 314 nm. These CD data are not very supportive of any secondary structure formation in dilute condition of the gelator assembly⁵⁷. However, from XRD and SAXS data are the suggestive of a β -sheet-like structure of an aggregated gel state. By combining the data obtained from NMR, FT-IR, SAXS and PXRD we propose a plausible molecular arrangement for 1:1 hydrogel shown in Fig. 8.

Drug release study

We examined the ability of the gels to encapsulate drugs and studied the release profiles. Among the three hydrogels, we chose the 1:1 hydrogel for the release profile as it is the best amongst others in respect of rheological stability. We tested release profiles with three drugs, amoxicillin, rifampicin, and doxorubicin. For this the two-component gelators (1:1 of 0.6% w/v) were dissolved in ultrapure water (600 μ l) for each drug. Then pre-prepared aqueous solutions of each drug (0.1 mg in 400 μ l ultrapure water) were added to the gelator solutions and kept for gelation. It was observed that stable hydrogels

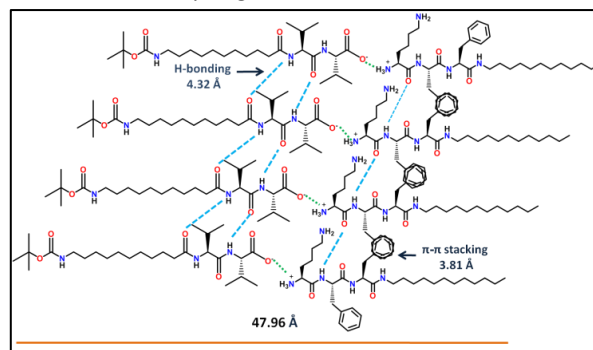


Fig. 8 Probable schematic model of model for packing arrangement of the gelator molecules.

were formed for each case and an aliquot (1 mL) of ultrapure water was added at the top of each hydrogel loaded with drugs to investigate the drug release profiles. Interestingly, all three drug-loaded hydrogels exhibited release profile and over the time of about 72 hours the release of amoxicillin, (Fig. 9a) rifampicin, (Fig. 9b) and doxorubicin (Fig. 9c) were monitored by UV-vis spectroscopic measurements at 25° C. In this case the data were recorded by monitoring UV-vis absorbance at 273 nm, 474 nm, and 480 nm for amoxicillin, rifampicin, and doxorubicin respectively.

The release profiles of amoxicillin and rifampicin are quite similar whether in the case of doxorubicin shows a more gradual release. In 10 h, 49% drug release was observed in the case of amoxicillin and 46% rifampicin was released in the same time period. In this duration the release is some extent fast. After 14 h the drug release was slowed down in both cases. The release continued up to 72 h and in this period, the

drug release reached 76% for amoxicillin and for rifampicin it reached 70%. However, in the case of doxorubicin, the release

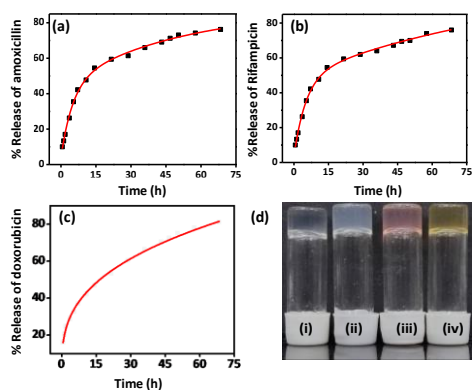


Fig. 9 Sustained release of (a) amoxicillin, (b) rifampicin, and (c) doxorubicin from 1:1 hydrogel. (d) Images of 1:1 hydrogels (i) without loaded drug, (ii) loaded with amoxicillin, (iii) loaded with doxorubicin, and (iv) loaded with rifampicin.

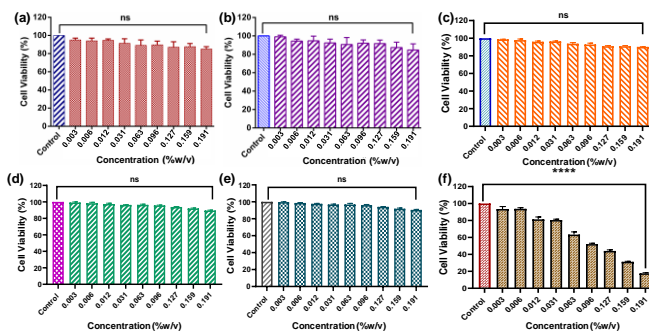
profile was not fast. For doxorubicin, 38% drug release was observed in 4 h. In the next 6 h it reached 39 % which was lesser than for the two antibiotic drugs. However, 46% release was observed after 14 h and after 72 h the drug release reached 81%. In each case, first order kinetics was observed as is clear from the data in Fig. S8 (ESI[†]).

Cytotoxicity Study

A material must be cytocompatible over a suitable range of concentrations for its *in vivo* practical use. We studied the cytocompatibility of the 1:1 hydrogel on the human embryonic kidney (HEK 293) and CHO (Chinese Hamster Ovary) cells. The cytotoxicity is usually assessed according to: non-cytotoxic (>90%), slight (60–90%), moderate (30–60%), and severe (<30%) with respect to control cells cultured in the same medium. Here, cytotoxicity of 1:1 hydrogel was determined using MTT assay for different concentrations (% w/v) of the gelators (Fig. 10) after 24 h incubation of each sample. Over the range of 1:1 hydrogel sample concentrations examined, no significant cytotoxicity was observed for the cell lines i.e. HEK-293, CHO and MDA-MB 231 triple negative breast cancer cells used in this experiment. For the HEK-293 cell, the cell viability was observed to be about 91% (Fig. 10a) and for the CHO cell, it was about 95% (Fig. 10b). In the case of cancer cell the cell viability was observed about 97% (Fig. 10c). However, the drug loaded hydrogels (for amoxicillin and rifampicin) also exhibited no significant cytotoxic effect on the cancer cells (Fig. 10d and 10e) and the cell viabilities were 94 and 95% respectively. The hydrogel loaded with doxorubicin showed significant cytotoxicity to the cancer cell. Here, the cancer cells survived only about 18% (Fig. 10e). From all these observations, it can be concluded that 1:1 hydrogel, amoxicillin and rifampicin loaded hydrogels are non-cytotoxic and thus have potential to be used in biological applications.

Conclusion

We have shown the formation of two-component hydrogel that can be formed easily by mixing the two components using a heat/cool method. This type of hydrogel enables the tuning of various properties including rheological characteristics, and morphological properties which can be used for different applications. The morphology is associated with the formation of single-component fibril assemblies for the 1:1 and 2:1



beamtime (ref. SM29895-1) and Charlotte Edwards-Gayle and Lucas de Mello for support. We are very thankful to Prof. Prosenjit Sen and Mr. Akash Chatterjee of IACS, Kolkata for helping in MTT assay study. We also thank Prof. Bishakh Bhattacharya of IIT, Kanpur, India for the helpful discussion about the manuscript.

Notes and References

- D. M. Raymond, B. L. Abraham, T. Fujita, M. J. Watrous, E. S. Toriki, T. Takano and B. L. Nilsson, *ACS Appl. Bio Mater.*, 2019, **2**, 2116–2124.
- M. J. S. Hill and D. J. Adams, *Soft Matter*, 2022, **18**, 5960–5965.
- B. Hansda, J. Majumder, B. Mondal, A. Chatterjee, S. Das, S. Kumar, R. Gachhui, V. Castelletto, I. W. Hamley, P. Sen and A. Banerjee, *Langmuir*, 2023, **39**, 7307–7316.
- B. Mondal, D. Bairagi, N. Nandi, B. Hansda, K. S. Das, C. J. C. Edwards-Gayle, V. Castelletto, I. W. Hamley and A. Banerjee, *Langmuir*, 2020, **36**, 12942–12953.
- E. Parisi, S. Adorinni, A. M. Garcia, S. Kralj, R. D. Zorzi and S. Marchesan, *J Pept Sci.*, 2023, e3524.
- A. Torres-Martínez, C. A. Angulo-Pachón, F. Galindo and J. F. Miravet, *Soft Matter*, 2019, **15**, 3565–3572.
- J. Omar, D. Ponsford, C. A. Dreiss, T. Lee and X. J. Loh, *Chem. Asian J.*, 2022, **17**, e202200081.
- A. Dawn, M. Mirzamani, C. D. Jones, D. S. Yufit, S. Qian, J. W. Steed and H. Kumari, *Soft Matter*, 2018, **14**, 9489–9497.
- J. M. Godbe, R. Freeman, J. A. Lewis, I. R. Sasselli, M. H. Sangji and S. I. Stupp, *Acta Biomater.*, 2021, **135**, 87–99.
- A. Jain, S. Dhiman, A. Dhayani, P. K. Vemula and S. J. George, *Nat. Commun.*, 2019, **10**, 450.
- N. Singh, A. Lopez-Acosta, G. J. M. Formon and T. M. Hermans, *J. Am. Chem. Soc.*, 2022, **144**, 410–415.
- P. D. Thornton, R. J. Mart and R. V. Ulijn, *Adv. Mater.*, 2007, **19**, 1252–1256.
- M. Yi, J. Guo, H. He, W. Tan, N. Harmon, K. Ghebreyessus and B. Xu, *Soft Matter*, 2021, **17**, 8590–8594.
- G. Ghosh, R. Barman, J. Sarkar and S. Ghosh, *J. Phys. Chem. B*, 2019, **123**, 5909–5915.
- A. Baral, S. Roy, S. Ghosh, D. Hermida-Merino, I. W. Hamley and A. Banerjee, *Langmuir*, 2016, **32**, 1836–1845.
- L. Xu, M. Zhang, X. Zhu, C. Xue, H. X. Wang and M. Liu, *ACS Appl. Mater. Interfaces*, 2022, **14**, 1765–1773.
- K. Gayen, K. Basu, D. Bairagi, V. Castelletto, I. W. Hamley and A. Banerjee, *ACS Appl. Bio Mater.*, 2018, **1**, 1717–1724.
- T. Shao, N. Falcone and H.-B. Kraatz, *ACS Omega*, 2020, **5**, 1312–1317.
- C. A. Angulo-Pachón, V. Pozo and J. F. Miravet, *J. Colloid Interface Sci.*, 2023, **635**, 524–534.
- K. Basu, A. Baral, S. Basak, A. Dehsorkhi, J. Nanda, D. Bhunia, S. Ghosh, V. Castelletto, I. W. Hamley and A. Banerjee, *Chem. Commun.*, 2016, **52**, 5045–5048.
- V. B. Kumar, B. Ozguney, A. Vlachou, Y. Chen, E. Gazit and P. Tamamis, *J. Phys. Chem. B*, 2023, **127**, 1857–1871.
- L. L. E. Mears, E. R. Draper, A. M. Castilla, H. Su, Zhuola, B. Dietrich, M. C. Nolan, G. N. Smith, J. Douth, S. Rogers, R. Akhtar, H. Cui and D. J. Adams, *Biomacromolecules*, 2017, **18**, 3531–3540.
- M. L. Jagrosse, P. Agredo, B. L. Abraham, E. S. Toriki and B. L. Nilsson, *ACS Biomater. Sci. Eng.*, 2023, **9**, 784–796.
- K. Nagy-Smith, Y. Yamada and J. P. Schneider, *J. Mater. Chem. B*, 2016, **4**, 1999–2007.
- J. E. P. Sun, B. Stewart, A. Litan, S. J. Lee, J. P. Schneider, S. A. Langhans and D. J. Pochan, *Biomater. Sci.*, 2016, **4**, 839–848.
- R. Martí-Centelles, I. Dolz-Pérez, J. De La O, I. Ontoria-Oviedo, P. Sepúlveda, V. J. Nebot, M. J. Vicent and B. Escuder, *ACS Appl. Bio Mater.*, 2021, **4**, 935–944.
- V. B. Kumar, O. S. Tiwari, G. Finkelstein-Zuta, S. Rencus-Lazar and E. Gazit, *Pharmaceutics*, 2023, **15**, 345.
- S. Koutsopoulos, *J. Biomed. Mater. Res. Part A*, 2016, **104**, 1002–1016.
- B. Mondal, V. K. Gupta, B. Hansda, A. Bhoumik, T. Mondal, H. K. Majumder, C. J. C. Edwards-Gayle, I. W. Hamley, P. Jaisankar and A. Banerjee, *Soft Matter*, 2022, **18**, 7201–7216.
- J. M. Godbe, R. Freeman, L. F. Burbulla, J. Lewis, D. Krainc and S. I. Stupp, *ACS Biomater. Sci. Eng.*, 2020, **6**, 1196–1207.
- B. Hansda, B. Mondal, S. Hazra and A. Banerjee, *J. Pept. Sci.*, 2023, e3492.
- C. Sahub, J. L. Andrews, J. P. Smith, M. A. Mohamad Arif, B. Tomapatanaget and J. W. Steed, *Mater. Chem. Front.*, 2021, **5**, 6850–6859.
- M. Maity and U. Maitra, *European J. Org. Chem.*, 2017, **2017**, 1713–1720.
- J. N. B. D. Pelin, B. B. Gerbelli, C. J. C. Edwards-Gayle, A. M. Aguilar, V. Castelletto, I. W. Hamley and W. A. Alves, *Langmuir*, 2020, **36**, 2767–2774.
- N. Nandi, A. Baral, K. Basu, S. Roy and A. Banerjee, *Pept. Sci.*, 2017, **108**, e22915.
- P. K. Gavel, N. Kumar, H. S. Parmar and A. K. Das, *ACS Appl. Bio Mater.*, 2020, **3**, 3326–3336.
- C. C. Piras, A. G. Kay, P. G. Genever, J. Fitremann and D. K. Smith, *Chem. Sci.*, 2022, **13**, 1972–1981.
- F. Sheehan, D. Sementa, A. Jain, M. Kumar, M. Tayarani-Najjaran, D. Kroiss and R. V. Ulijn, *Chem. Rev.*, 2021, **121**, 13869–13914.
- C. C. Piras, C. S. Mahon, P. G. Genever and D. K. Smith, *ACS Biomater. Sci. Eng.*, 2022, **8**, 1829–1840.
- D. Bairagi, P. Biswas, K. Basu, S. Hazra, D. Hermida-Merino, D. K. Sinha, I. W. Hamley and A. Banerjee, *ACS Appl. Bio Mater.*, 2019, **2**, 5235–5244.
- P. Qin, Z. Wu, P. Li, D. Niu, M. Liu and M. Yin, *ACS Appl. Mater. Interfaces*, 2021, **13**, 18047–18055.
- T. J. Cotey, H. Sai, C. Perez, L. C. Palmer and S. I. Stupp, *Soft Matter*, 2021, **17**, 4949–4956.
- A. K. Patterson and D. K. Smith, *Chem. Commun.*, 2020, **56**, 11046–11049.
- B. Pramanik, S. Ahmed, N. Singha, B. K. Das, P. Dowari and D. Das, *Langmuir*, 2019, **35**, 478–488.
- Y. Sun, L. A. Bentolila and T. J. Deming, *ACS Macro Lett.*, 2019, **8**, 1275–1279.
- J. K. Sahoo, M. A. Vandenberg, E. E. Ruiz Bello, C. D. Nazareth and M. J. Webber, *Nanoscale*, 2019, **11**, 16534–16543.
- N. Singh, K. Zhang, C. A. Angulo-Pachón, E. Mendes, J. H. Van Esch and B. Escuder, *Chem. Sci.*, 2016, **7**, 5568–5572.
- S. Dahan, P. Aibinder, B. Khalfin, J. Moran-Gilad and H. Rapaport, *ACS Biomater. Sci. Eng.*, 2023, **9**, 352–362.

- 49 R. Martí-Centelles, I. Dolz-Pérez, J. De la O, I. Ontoria-Oviedo, P. Sepúlveda, V. J. Nebot, M. J. Vicent and B. Escuder, *ACS Appl. Bio Mater.*, 2021, **4**, 935–944.
- 50 B. O. Okesola, Y. Wu, B. Derkus, S. Gani, D. Wu, D. Knani, D. K. Smith, D. J. Adams and A. Mata, *Chem. Mater.*, 2019, **31**, 7883–7897.
- 51 M. Ghosh, M. Halperin-Sternfeld, I. Grigoriants, J. Lee, K. T. Nam and L. Adler-Abramovich, *Biomacromolecules*, 2017, **18**, 3541–3550.
- 52 J. Gao, C. Tang, M. A. Elsayy, A. M. Smith, A. F. Miller and A. Saiani, *Biomacromolecules*, 2017, **18**, 826–834.
- 53 E. Prince and E. Kumacheva, *Nat. Rev. Mater.*, 2019, **4**, 99–115.
- 54 A. N. Shy, H. Wang, Z. Feng and B. Xu, *Molecules*, 2020, **26**, 77.
- 55 T. Gorai and U. Maitra, *Angew. Chemie - Int. Ed.*, 2017, **56**, 10730–10734.
- 56 C. J. C. Edwards-Gayle, N. Khunti, I. W. Hamley, K. Inoue, N. Cowieson and R. Rambo, *Journal of Synchrotron Radiation*, 2021, **28**, 318–321.
- 57 V. Castelletto, C. J. C. Edwards-Gayle, F. Greco, I. W. Hamley, J. Seitsonen, and J. Ruokolainen, *ACS Appl. Mater. Interfaces*, 2019, **11**, 33573–33580.